magnetochemistry

MDPI

Article

Magneto-Structural Relationship of Tetragonally-Compressed Octahedral Iron(II) Complex Surrounded by a *pseudo-S*$_6$ Symmetric Hexakis-Dimethylsulfoxide Environment

Hiroshi Sakiyama [1,*], Takaaki Abiko [1], Masayuki Koikawa [2] and Mikio Yamasaki [3]

[1] Department of Science, Faculty of Science, Yamagata University, 1-4-12 Kojirakawa, Yamagata 990-8560, Japan; soften_abiko0325@yahoo.co.jp
[2] Department of Chemistry and Applied Chemistry, Faculty of Science and Engineering, Saga University, 1 Honjo-machi, Saga 840-8502, Japan; koikawa@cc.saga-u.ac.jp
[3] Application Laboratories, Rigaku Corporation, Matsubara 3-9-12, Akishima, Tokyo 196-8666, Japan; yamasaki@rigaku.co.jp
* Correspondence: saki@sci.kj.yamagata-u.ac.jp

Abstract: Since the octahedral high-spin iron(II) complex has the $^5T_{2g}$ ground term, the spin-orbit coupling should be considered in magnetic analysis; however, such treatment is rarely seen in recent papers, although the symmetry-sensitive property is of interest to investigate in detail. A method to consider the *T*-term magnetism was well constructed more than half a century ago. On the other hand, the method has been still improved in recent years. In this study, the octahedral high-spin iron(II) complex $[Fe(dmso)_6][BPh_4]_2$ (dmso: dimethylsulfoxide) was newly prepared, and the single-crystal X-ray diffraction method revealed the tetragonal compression of the D_4-symmetric coordination geometry around the iron(II) ion and the *pseudo-S*$_6$ hexakis-dmso environment. From the magnetic data, the sign of the axial splitting parameter, Δ, was found to be negative, indicating the ^5E ground state in the D_4 symmetry. The DFT computation showed the electronic configuration of $(d_{xz})^2(d_{x^2-y^2})^1(d_{yz})^1(d_{xy})^1(d_{z^2})^1$ due to the tetragonal compression and the *pseudo-S*$_6$ environment of dmso π orbitals. The electronic configuration corresponded to the ^5E ground term, which was in agreement with the negative Δ value. Therefore, the structurally predicted ground state was consistent with the estimation from the magnetic measurements.

Keywords: octahedral high-spin iron(II) complex; crystal structure; magnetic properties; density functional theory; magneto-structural relationship

Citation: Sakiyama, H.; Abiko, T.; Koikawa, M.; Yamasaki, M. Magneto-Structural Relationship of Tetragonally-Compressed Octahedral Iron(II) Complex Surrounded by a *pseudo-S*$_6$ Symmetric Hexakis-Dimethylsulfoxide Environment. *Magnetochemistry* **2021**, *7*, 30. https://doi.org/10.3390/magnetochemistry7020030

Academic Editor: Donatella Armen-tano

Received: 29 January 2021
Accepted: 18 February 2021
Published: 23 February 2021

1. Introduction

Octahedral high-spin iron(II) complexes have the $^5T_{2g}$ ground terms, and their fundamental magnetic theory was constructed in the 1960s and 1970s [1–3]. On the other hand, the theory does not seem to be often used recently, probably because the contribution of the orbital angular momentum is difficult to be treated. However, consideration of the spin-orbit coupling is important for understanding the correct electronic state, which leads to an excellent physical property prediction and material design. In this article, for the purpose of showing how to analyze magnetic data of octahedral high-spin iron(II) complexes, we introduce some of the improved new techniques: (1) How to determine the sign of the ligand field splitting, (2) how to simulate field-effect in the low-temperature region, and (3) how to simulate saturation behavior of magnetization.

Metal complexes possessing the *T*-term ground states often show unusual magnetic behavior due to the spin-orbit coupling. After Kotani proved the contribution of the spin-orbit coupling for such compounds [4], the effects of the low-symmetry ligand field and

the orbital reduction factor were found to play an important role [5–8], and the temperature dependence of the effective magnetic moment came to be successfully simulated for mononuclear *T*-ground-term complexes [2,7,8]. Here, we want to emphasize that the spin-orbit splitting caused by the spin–orbit interaction is different from the normal zero-field splitting. The normal zero-field splitting is caused by the spin–spin interaction when the number of unpaired electrons is equal to or larger than two. The spin-orbit splitting is actually a splitting in the zero-field, but is caused by the spin-orbit coupling when the orbital angular momentum remains unquenched. The magnetic behavior caused by the spin-orbit splitting is sometimes approximately analyzed by the theory of zero-field splitting, but it is just an approximation and the data should be analyzed by the theory considering the spin-orbit coupling.

For the octahedral high-spin iron(II) complexes, Griffiths obtained a 15 × 15 secular matrix for the ${}^5T_{2g}$ term [1], considering the spin-orbit coupling. He obtained an energy diagram of the 15 states from the ${}^5T_{2g}$ term with respect to the distortion around the iron(II) ion. Figgis also derived the secular matrix for the ${}^5T_{2g}$ term and successfully simulated the temperature dependence of the effective magnetic moment [2]. Later, Long introduced the orbital reduction factor for the octahedral high-spin iron(II) complexes [3]. Recently, single-ion magnet behavior was observed in high-spin iron(II) complexes [9,10], although they are not octahedral, and the interests to the high-spin iron(II) complexes are increasing. The study on the magneto-structural relationship is expected to give important insight in designing magnetic materials.

When using the theory for the ${}^2T_{2g}$-ground term complexes [1–3], the 15 × 15 secular matric were to be solved each time for an octahedral high-spin iron(II) complex. However, recently, the secular matrix was successfully solved to obtain Zeeman energy equations expressed as the functions of three independent parameters, Δ, λ, and κ, where Δ is the axial ligand-field splitting parameter, λ is the spin–orbit coupling parameter, and κ is the orbital reduction factor [11]. With these Zeeman energy equations, magnetic simulation can be performed by simply substituting numerical values for parameters without solving the secular matrix each time. In this study, magnetic analysis was conducted for a newly prepared octahedral high-spin iron(II) complex, $[Fe(dmso)_6][BPh_4]_2$ (dmso: dimethylsulfoxide), using the equations, for the purpose of gaining further insight into magneto-structural relationship.

2. Results and Discussion

*2.1. Crystal Structure of **1***

Crystal structure of $[Fe(dmso)_6][BPh_4]_2$ (**1**) was determined by the single-crystal X-ray method. Crystallographic data are summarized in Table 1, and the structures of the complex cation, $[Fe(dmso)_6]^{2+}$, are shown in Figure 1. The compound consists of the complex cations and the tetraphenyl borate anions in a 1:2 molar ratio. In the complex cation, the six dmso molecules coordinate to the central iron(II) ion through oxygen atoms, forming an octahedral coordination geometry with the O_6 donor set. The cation is centrosymmetric, and tetragonally compressed along the Fe(1)-O(7) direction. The bond distances, Fe(1)-O(5), Fe(1)-O(6), and Fe(1)-O(7), were 2.1408(7), 2.1586(9), and 2.0899(8) Å, respectively. The central FeO_6S_6 unit can be approximated as the S_6 symmetry (Figure 1a). Four inter-ligand CH···O hydrogen bonds were found in a complex cation (Figure 1b), affording a 16-membered chelating ring perpendicular to the tetragonal compression axis. Earlier, the crystal structure of $[Fe(dmso)_6][SnCl_6]_2$ (**2**) was reported [12], and phase transition behavior was investigated for $[Fe(dmso)_6][ClO_4]_2$ [13], but complex **1** has not been reported so far.

Table 1. Crystallographic data and refinement parameters of **1**.

Empirical Formula	$C_{60}H_{76}B_2FeO_6S_6$
Formula Weight	1163.08
Crystal system	tetragonal
Space group	$P4_2/n$
a/Å	17.76361(7)
c/Å	19.46383(12)
V/Å^3	6141.73(5)
Z	4
Crystal Dimensions/mm	0.373 × 0.292 × 0.211
T/K	203
λ/Å	0.71073
ρ_{calcd}/g cm^{-3}	1.528
μ/mm^{-1}	0.496
F(000)	2464
$2\theta_{max}$/°	60.1
No. of Reflections Measured	173,887
No. of independent reflections	8991 (Rint = 0.0201)
Data/restraints/parameters	8991/163/405
R_1 [a] (I > 2.00σ(I))	0.0327
wR_2 [b] (All reflections)	0.0356
Goodness of Fit Indicator	1.029
Highest peak, deepest hole/e Å^{-3}	0.49, −0.47
CCDC deposition number	1854569

[a] $R_1 = \Sigma||Fo| - |Fc||/\Sigma|Fo|$, [b] $wR_2 = [\Sigma(w(Fo^2 - Fc^2)^2)/\Sigma w(Fo^2)^2]^{1/2}$.

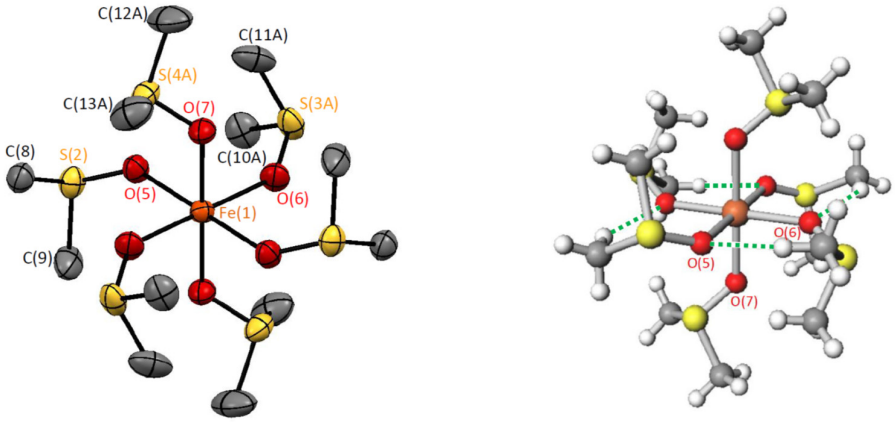

(**a**) (**b**)

Figure 1. Crystal structures of $[Fe(dmso)_6]^{2+}$ at 203 K: (**a**) With atom labelling and (**b**) with hydrogen-bonds marked as green dot line. Disordered minor structures are omitted for clarity.

Among the six dmso moieties of the $[Fe(dmso)_6]^{2+}$ complex cation in **1**, four of them were found to be disordered, suggesting the sulfur-inversion motion as well as the cobalt(II) and zinc(II) derivatives [14,15]. Among the crystals of $[Co(dmso)_6][BPh_4]_2$, $[Zn(dmso)_6][BPh_4]_2$, $[Mg(dmso)_6][BPh_4]_2$ [16], and $[Fe(dmso)_6][BPh_4]_2$ (**1**) complexes, the cobalt(II) and zinc(II) complexes form isomorphous crystals, while the iron(II) complex (**1**) is isomorphous to the magnesium (II) complex. In the magnesium (II) complex cation, a tetragonal compression was observed similar to **1**.

In the related iron(II) complex **2**, the $[Fe(dmso)_6]^{2+}$ cation was more symmetrical than that in **1**, and the cation in **2** exactly belongs to the S_6 point group. Each dmso moieties in **2** showed the similar disorder at 213 K, suggesting the sulfur-inversion motion in the crystal. The Fe-O distances in **2** [2.121(3) Å] was comparable to the average Fe-O distance in **1** [2.1298(8) Å]. In **2**, the octahedral FeO_6 coordination geometry showed the slight trigonal compression along the S_6 axis. Using the conformation notation in reference 16, the conformer of the main $[Fe(dmso)_6]^{2+}$ structure in **2** was the "α_6" conformation, which was considered to be the most stable one. On the other hand, the conformer of the main $[Fe(dmso)_6]^{2+}$ structure in **1** was "*trans*-$\beta_2\gamma_4$" conformation, which was not so stable on its own. The reason for this unstable conformation is considered to be due to the crystal-packing effect of the bulky tetraphenylborate anions [15–17] as discussed in our previous paper on $[Mg(dmso)_6][BPh_4]_2$ [16].

In the crystal structure of **1**, the complex cation was surrounded by eight tetraphenylborate anions, and the distinct CH···π interactions were observed between the dmso methyl groups and the phenyl rings of the tetraphenylborate anions.

2.2. Magnetic Properties

Magnetic susceptibility (χ_A) was measured in the temperature range of 2–300 K, and the $\chi_A T$ *versus* T plot is shown in Figure 2. The observed $\chi_A T$ value at 300 K (3.46 cm^3 K mol^{-1}) was larger than the spin-only value for the $S = 2$ state (3.00 cm^3 K mol^{-1}), and this suggests a contribution of the orbital angular momentum. When lowering the temperature, the observed $\chi_A T$ value slightly increased until at 120 K (3.47 cm^3 K mol^{-1} at 120 K), and decreased until at 2 K (1.42 cm^3 K mol^{-1} at 2 K). This behavior, possessing a $\chi_A T$ maximum, is typical of $^5T_{2g}$-term magnetism for octahedral high-spin iron(II) complexes [2].

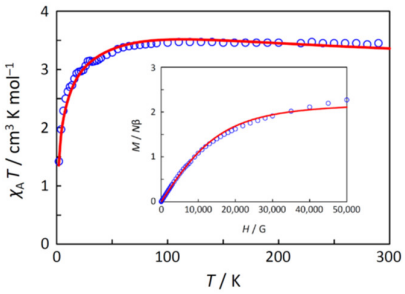

Figure 2. The χT versus T plot and the M versus H plot (insertion). The observed data (◦) and the theoretical curves (–) with the best-fitting parameter set (λ, κ, v, θ) = (−100 cm^{-1}, 0.66, 5.5, −1.5 K).

Three typical theoretical curves are depicted in Figure 3, based on the Hamiltonian, $\mathbf{H} = \Delta(\mathbf{L}_z^2 - 2/3) + \kappa\lambda\mathbf{L}\cdot\mathbf{S} + \beta(\kappa\mathbf{L}_u + g_e\mathbf{S}_u)\cdot H_u$ ($u = x, y, z$) [11], where Δ is the axial splitting parameter, κ is the orbital reduction factor, and λ is the spin-orbit coupling parameter. In addition, the axiality parameter v, defined as $v = \Delta/(\kappa\lambda)$, was introduced, and a relationship can be seen between the v value and the maximum $\chi_A T$ temperature (T_{max}). That is, the larger the v value, the higher the maximum temperature, T_{max}. When the T_{max} value is in the range of 138–150 K, the $|v|$ value is considered to be close to zero; when the T_{max} value is lower than 138 K, the v value is considered to be positive; when the T_{max} value is higher than 150 K, the v value is considered to be negative. Therefore, since the T_{max} value of the observed data is ~120 K, the v value is considered to have a positive sign and the Δ value is considered to be negative, indicating the ^5E ground state (Figure 4). That is, the $^5T_2$ ground term in the O symmetry splits into ^5E and $^5B_2$ terms in the D_4 symmetry, and the ^5E term is lower in energy than the $^5B_2$ term.

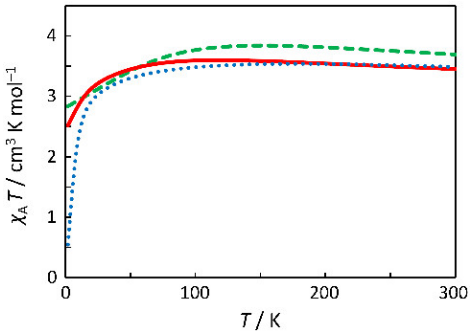

Figure 3. Theoretical χT *versus* T curves with Δ = −350 cm^{-1} (v = 5) (—), Δ = 0 cm^{-1} (v = 0) (– – –), and Δ = +350 cm^{-1} (v = −5) (·····) and with fixed parameters (λ, κ) = (−100 cm^{-1}, 0.70).

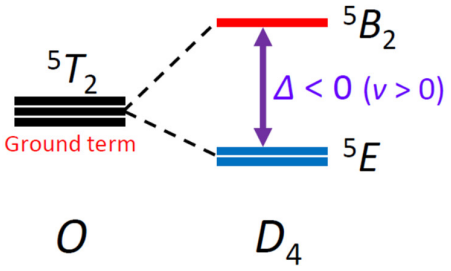

Figure 4. Energy diagram of the ground terms for the octahedral high-spin iron(II) complex.

In the earlier works [1–3], the Hamiltonian had been slightly being modified with respect to handling the orbital reduction factor. Figgis and coworkers introduced the orbital reduction factor in the third term (Zeeman term) of the Hamiltonian [2], and Long and coworker further introduced the orbital reduction factor in the second term (spin-orbit coupling term) of the Hamiltonian [3]. Long and coworker used a parameter $v = \Delta/\lambda$, but in this study, we used the axiality parameter $v = \Delta/(\kappa\lambda)$ [11], because it has some advantages in expressing coefficients. It is noted that Kahn used a parameter $v = \Delta/|\lambda|$ for an octahedra high-spin cobalt(II) complexes [18]. Since our treatment is slightly different from the others, the simulation results are also slightly different from the earlier works.

Using the Figgis basis set [2] for the $^5T_{2g}$ term, the secular matrices were constructed [11]. The shapes of the resulting matrices are essentially the same as the Griffiths matrices [1] except for the orbital reduction factor. The exact solution was successfully obtained for the matrices [11], and the zero-field energies and the first- and the second-order Zeeman coefficients were obtained for 15 sub-states of the $^5T_{2g}$ term. The zero-field magnetic susceptibility was obtained as the ordinary Van Vleck equation, and in addition, the field-dependent magnetic susceptibility equation was obtained as expressed in Equations (1)–(3).

$$\chi_{A,av} = \frac{\chi_z + 2\chi_x}{3}, \quad (1)$$

$$\chi_{A,u} = \frac{N\sum_n\left(-E^{(1)}_{n,u} - 2E^{(2)}_{n,u}H_u\right)\exp(-E_{n,u}/kT)}{H_u\sum_n \exp(-E_{n,u}/kT)} \quad (u = z, x; n = 1\text{–}15), \quad (2)$$

$$E_{n,u} = E^{(0)}_{n,u} + E^{(1)}_{n,u}H_u + E^{(2)}_{n,u}H_u^2 \quad (u = z, x; n = 1\text{–}15), \quad (3)$$

The powder average of the magnetization is generally expressed by Equation (4). In this study, the expanded equation [Equation (5) with Equation (6)] [19] by calculating the integrals for the axial symmetry was used. We calculated the powder average of the magnetization using Equation (7) with m = 90.

$$M_{av} = (4\pi)^{-1}\int_0^{2\pi}\int_0^{\pi} M(\theta,\varphi)\sin\theta\, d\theta d\varphi, \quad (4)$$

$$M_{\mathrm{av}} = \lim_{m\to\infty} \sum_{j=1}^{m} M\left(\frac{\left(j-\frac{45}{m}\right)\pi}{180}\right)\left[\cos\frac{(j-1)\pi}{180} - \cos\frac{j\,\pi}{180}\right], \quad (5)$$

$$M(\theta) = \frac{N\sum_n\left(-E_{n,\theta}^{(1)} - 2E_{n,\theta}^{(2)}H_\theta\right)\exp\left(-E_{n,\theta}/kT\right)}{\sum_n \exp\left(-E_{n,\theta}/kT\right)}, \quad (6)$$

$$M_{\mathrm{av}} = \sum_{j=1}^{m} M\left(\frac{\left(j-\frac{45}{m}\right)\pi}{180}\right)\left[\cos\frac{(j-1)\pi}{180} - \cos\frac{j\,\pi}{180}\right], \quad (7)$$

In the analysis, at first, the $\chi_A T$ *versus* T data in the range of 10–300 K were analyzed by the zero-field equation (Figure S1), and the obtained parameter set was obtained as (λ, κ, v) = (−100 cm^{-1}, 0.66, 5.6) with the discrepancy factors of R_χ = 3.9 × 10^{-3} and $R_{\chi T}$ = 1.6 × 10^{-3} in the range of 10–300 K, and R_χ = 2.4 × 10^{-1} and $R_{\chi T}$ = 5.1 × 10^{-3} in the range of 2–300 K. The Δ value was calculated to be −370 cm^{-1}. The obtained λ value is consistent with the −ζ/4 value with ζ = 400 cm^{-1} for iron(II) ion [20], where ζ is the single-electron spin-orbit coupling parameter. The small κ value is thought to be due to the π orbital interaction with the dmso ligands, which will be discussed in the following density functional theory (DFT) computation section. The obtained positive v value is consistent with the initial estimation from the $\chi_A T$ *versus* T curve. The data in the range of 10–300 K were well reproduced with reasonable parameters; however, the decrease in $\chi_A T$ below 10 K and the magnetization were not reproduced.

For the decrease in $\chi_A T$, in this case, there are two possible reasons, the field-saturation effect and the intermolecular antiferromagnetic interactions. If the magnetic field effect of 3000 Oe was considered, using the field-dependent susceptibility equation [Equations (1)–(3)], the obtained parameter set was the same, but the discrepancy factors became slightly better (R_χ = 3.8 × 10^{-3} and $R_{\chi T}$ = 1.5 × 10^{-3} in the range of 10–300 K; R_χ = 2.4 × 10^{-1} and $R_{\chi T}$ = 4.3 × 10^{-3} in the range of 2–300 K). By the field effect of 3000 Oe, the calculated $\chi_A T$ value became 6% smaller at 2 K, and 1.5% smaller at 4 K Therefore, the small contribution of field-saturation effect was confirmed, indicating that the field-saturation effect was not dominant in the $\chi_A T$ decrease.

In the next approach, the intermolecular interaction was also considered in addition to the field effect, introducing the Weiss constant, θ, for the intermolecular interaction. The full $\chi_A T$ versus T data (2–300 K) and the field-dependent data of the magnetization were simultaneously analyzed, and both data were successfully fitted as shown in Figure 2. The best-fitting parameter set was obtained as (λ, κ, v, θ) = (−100 cm^{-1}, 0.66, 5.5, −1.5 K) at H = 3000 Oe, with discrepancy factors of R_χ = 2.6 ×10^{-3} and $R_{\chi T}$ = 4.3 ×10^{-4} (in the full temperature range). The Δ value was calculated to be −363 cm^{-1}, and the obtained θ value corresponded to zJ = ~−0.5 cm^{-1}. The zJ value is consistent with the intermolecular antiferromagnetic interaction through CH···π interactions observed in the crystal structure. Both the full $\chi_A T$ versus T data and the field dependent data of the magnetization were successfully analyzed with reasonable parameters, and the intermolecular interaction was found to be the dominant factor for the decrease in $\chi_A T$ below 10 K.

Using the Figgis basis set [2], the lowest three states from the $^5T_{2g}$ term are described by the wave functions expressed in Equations (8)–(10), where $|M_L, M_S\rangle$ (M_L = 0, ±1, ±2 and M_S = 0, ±1, ±2) are wave functions and c_k (k = 0 − 35) are coefficients. It is noted that the coefficients c_k depend only on two parameters κ and v. When the Δ value is negative, the ground state corresponds to the wave functions Ψ_2 and Ψ_3, and the coefficients c_4 and c_7 will be dominant. Therefore, the ground state can be approximated as the M_S = ±2 states. This enables us to calculate the g values of the ground state from the first-order Zeeman coefficients as g_z = 2.21 and g_x = 0.00, although these values are not ascertained by the electron spin resonance (ESR), because the compound is unfortunately ESR-silent. Further investigation has not been conducted on the single molecule magnet properties.

$$\Psi_1 = c_1|1,1\rangle + c_2\frac{\sqrt{2}}{2}\{|2,0\rangle - |-2,0\rangle\} + c_3|-1,-1\rangle, \quad (8)$$

$$\Psi_2 = c_4|1,2\rangle + c_5\frac{\sqrt{2}}{2}\{|2,1\rangle - |-2,1\rangle\} + c_6|-1,0\rangle, \quad (9)$$

$$\Psi_3 = c_7|-1,-2\rangle + c_8\frac{\sqrt{2}}{2}\{|2,-1\rangle - |-2,-1\rangle\} + c_9|1,0\rangle, \quad (10)$$

2.3. Density Functional Theory (DFT) Computation

The restricted open-shell Hartree-Fock (ROHF) DFT calculation was conducted for the $[Fe(dmso)_6]^{2+}$ complex cation, using the crystal structure. The ROHF calculation is suitable for considering *d*-orbitals with unpaired electrons. The energy levels of five molecular orbitals related to the *d*-orbitals are shown in Figure 5 together with the depiction of the molecular orbitals. The tetragonal compression axis was taken as the principal axis along the *z* direction. The *x* and *y* axes were taken along the two bisecting directions of the adjacent equatorial donor atoms, because the dmso π orbitals were considered to be oriented parallel to the bisecting directions. Therefore, the resulting d_σ orbitals are d_{z^2} and d_{xy}, and the d_π orbitals are $d_{x^2-y^2}$, d_{xz}, and d_{yz}. From the calculation, the d_{xz} orbital was found to be the lowest among the five *d*-orbitals and to be filled with two electrons, whereas other four orbitals were found to be singly occupied. The energy level of the lowest d_{xz} orbital may look unusually low compared with the *d-d* separation in the octahedral coordination geometry, but this is normal because only this orbital is doubly occupied. The order of the d_σ orbitals were $d_{xy} < d_{z^2}$, and this is consistent with the tetragonal compression along the *z* axis. From the point of view of the crystal field theory, the splitting of the d_π orbitals is not so much because the tetragonal compression is very small in this case and the effect of the π orbitals is generally less than 10% of the σ orbital. The order of the calculated d_π orbitals were $d_{xz} < d_{x^2-y^2} < d_{yz}$, and this seems to be consistent with the orientation of the dmso π orbitals arranged in the *pseudo*-S_6 symmetry. That is, the larger the overlap between the *d*-orbital and the dmso π orbitals, the higher in energy. Therefore, the electronic configuration becomes $(d_{xz})^2(d_{x^2-y^2})^1(d_{yz})^1(d_{xy})^1(d_{z^2})^1$, and this electronic configuration is consistent with the combination of the tetragonal compression and the orientation of the *pseudo*-S_6 symmetric dmso π orbital environment. The small orbital reduction factor (κ = 0.66), estimated from the magnetic data, was shown to be consistent with the significant interaction with the dmso π orbitals. Since the (d_{xz}, d_{yz}) orbitals in the tetragonally compressed D_4 coordination geometry were filled with three electrons, the ground state became ^5E in the D_4 approximation. This is consistent with the negative Δ value found from the magnetic analysis.

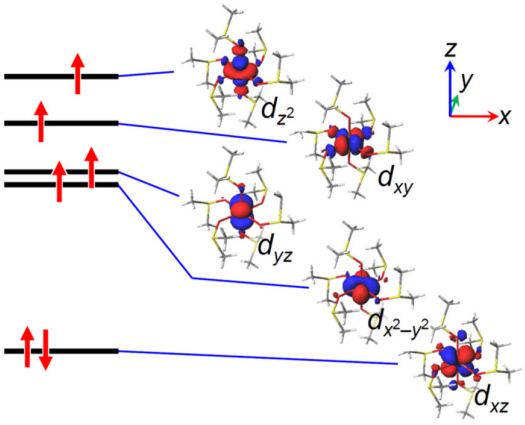

Figure 5. Energy levels and molecular orbitals obtained by the DFT calculation (LC-BOP/def2-tzvp).

2.4. Magneto-Structural Relationship

Now we discuss the magneto-structural relationship especially between the structure and the Δ value. In the crystal structure, the tetragonal compression was observed; however, the order of the d_π orbitals was found to be determined by the orientation of the dmso π orbitals, which was significantly influenced by the orientation of the dmso moieties. In this complex cation, the central iron(II) ion was surrounded by the *pseudo*-S_6 symmetric hexakis-dmso environment, and the combination of the tetragonal compression and the *pseudo*-S_6 environment was found to generate the *d*-orbital splitting in Figure 5, generating the electronic configuration of $(d_{xz})^2(d_{x^2-y^2})^1(d_{yz})^1(d_{xy})^1(d_{z^2})^1$. In the ideal D_4 symmetric coordination geometry due to the tetragonal-compression, the (d_{xz}, d_{yz}) orbitals are degenerate. However, in the (d_{xz}, d_{yz}) orbitals, the d_{xz} orbital becomes lower in energy due to the less overlap with the dmso π orbitals, and the (d_{xz}, d_{yz}) orbitals became filled with three electrons. This electronic configuration corresponded to the ^5E ground state in the D_4 symmetric coordination geometry. The ^5E ground state directly indicated the negative Δ value, which was consistent with the magnetic measurements. Judging from the negative sign of the Δ value, the magnetic anisotropy is considered to be uniaxial, and the tetragonal compression axis (*z* axis) is considered to be the easy axis.

In the case of the related cobalt(II) complex, $[Co(dmso)_6][BPh_4]_2$ [14], tetragonal elongation (along the *z* axis) was observed, and judging from the large orbital reduction factor, close to the free-ion value, the effect of the dmso π orbitals was thought to be smaller than that in the present iron(II) complex. The *pseudo*-degenerate (d_{xz}, d_{yz}) orbitals in the cobalt(II) complex were considered to be higher than the d_{xy} orbital, affording the ^4E ground state. This leads to the negative Δ value and the easy-axis anisotropy along the *z* axis.

3. Materials and Methods

3.1. Materials and Methods

All the chemicals were commercial products and were used as supplied. Elemental analyses (C, H, and N) were obtained on Elemental Analyzers, Yanaco (Tokyo, Japan) CHN Corder MT-5 and MT-6, at the Elemental Analysis Service Centre of Kyushu University (Fukuoka, Japan). IR spectra were recorded on a JASCO (Tokyo, Japan) FT/IR-4100 FT-IR spectrometer. Differential scanning calorimetry (DSC) measurements were conducted on PerkinElmer DSC 8500 in the temperature range of 303–203 K at scan rate of 30, 10, 5, and 1 K/min. Magnetic susceptibility measurements were made on Quantum Design (San Diego, CA, USA) MPMS XL5min SQUID susceptometer with scan rates of 10.0 K /min for 40–300 K and 0.5 K/min 2–40 K at 0.3 T. The isothermal magnetization was measured on Quantum Design MPMS XL5min SQUID susceptometer at 2 K in an applied field of 0–5 T. The magnetic correction for the sample holder was performed by measurement for the empty capsule. The susceptibilities were corrected for the diamagnetism of the constituent atoms using Pascal's constant.

3.2. Synthetic Procedures

$[Fe(dmso)_6][BPh_4]_2$ (**1**). Deoxygenated solvents were beforehand prepared by bubbling with nitrogen, and all operations were carried out under nitrogen. Iron(II) sulfate—water (1/7) (0.84 g, 3.0 mmol) was dissolved in hot water (1 mL), and to this was added dmso (3 mL) and 2-propanol solution (6 mL) of sodium tetraphenylborate (2.1 g, 6.1 mmol). The solution was refluxed for 20 min, and after the addition of 2-propanol (4 mL), the suspension was refluxed for 10 min to obtain white microcrystals. Recrystallized from hot dmso/2-propanol. Yield: 0.84 g (24%) (Found: C, 61.60; H, 6.45; Fe, 5.0%. Calc. for $C_{60}H_{76}B_2FeO_6S_6$ (1): C, 61.95; H, 6.60; Fe, 4.80%). Selected IR data [$\tilde{\nu}$/cm^{-1}] using a KBr disk: 3055-2910, 1578, 1476, 1425, 1314, 1151, 1011, 998, 949, 740, 705, 611.

3.3. Crystallography

Colorless single-crystals suitable for X-ray analysis were obtained by slow diffusion of 2-propanol to a dmso solution of **1** under nitrogen. Single-crystal diffraction data were measured on a Rigaku (Tokyo, Japan) XtaLAB PRO MM007 diffractometer. The structure was solved by direct methods and expanded using Fourier techniques. The non-hydrogen atoms were refined anisotropically except for the disordered dmso ligand, and hydrogen atoms were refined using the riding model. The final cycle of full-matrix least squares refinement on F_2 was let to satisfactory converge with $R_1 = 0.0327$ [$I > 2\sigma(I)$]. Final $R(F)$, $wR(F_2)$, and goodness of fit agreement factors, as well as details on data collection and analysis are in Table 1.

3.4. Computations

Magnetic analyses and magnetic simulation were conducted using MagSaki(FeII, β0.2.3) program of MagSaki series. The DFT computations were performed using GAMESS program [21,22] on Fujitsu PRIMERGY CX2550/CX2560 M4 (ITO super computer system) at Kyushu University. Structural optimizations were conducted with LC-BOP/def2-tzvp [23–25].

4. Conclusions

The octahedral high-spin iron(II) complex $[Fe(dmso)_6][BPh_4]_2$ (**1**) was newly prepared, and the single-crystal X-ray diffraction method revealed the tetragonal compression of the D_4-symmetric coordination geometry around the iron(II) ion and the *pseudo*-S_6 hexakis-dmso environment. From the magnetic data, the sign of the axial splitting parameter, Δ, was found to be negative, indicating the ^5E ground state in the D_4 symmetry. That is, the $^5T_2$ ground term in the O symmetry splits into ^5E and $^5B_2$ terms in the D_4 symmetry, and the ^5E term is lower in energy than the $^5B_2$ term. The DFT computation showed the electronic configuration of $(d_{xz})^2(d_{x^2-y^2})^1(d_{yz})^1(d_{xy})^1(d_{z^2})^1$ due to the tetragonal compression and the *pseudo*-S_6 environment of dmso π orbitals. The electronic configuration corresponded to the ^5E ground term, which was in agreement with the negative Δ value. Therefore, the structurally predicted ground state was consistent with the estimation from the magnetic measurements.

Supplementary Materials: The following are available online at www.mdpi.com/2312-7481/7/2/30/s1, Figure S1: The χT *versus* T plot and the M *versus* H plot (insertion).

Author Contributions: Conceptualization, H.S.; methodology, H.S.; software, H.S.; validation, H.S. and M.K.; formal analysis, H.S., T.A., M.K. and M.Y.; investigation, H.S. and T.A.; resources, H.S. and T.A.; data curation, H.S.; writing—original draft preparation, H.S. and M.K.; writing—review and editing, H.S. and M.Y.; visualization, H.S.; supervision, H.S.; project administration, H.S.; funding acquisition, H.S. All authors have read and agreed to the published version of the manuscript.

Funding: Please add: This research was funded by Japan society for the promotion of science (JSPS) KAKENHI, grant number 15K05445.

Data Availability Statement: The crystallographic data are available from the Cambridge Crystallographic Data Centre (CCDC). Other data not presented in Supplementary Materials are available on request from the corresponding author.

Conflicts of Interest: The authors declare no conflict of interest. The funders had no role in the design of the study; in the collection, analyses, or interpretation of data; in the writing of the manuscript, or in the decision to publish the results.

References

1. Griffith, J.S. *The Theory of Transition-Metal Ions*; Cambridge University Press: Cambridge, UK, 1961.
2. Figgis, B.N.; Lewis, J.; Mabbs, F.E.; Webb, G.A. The magnetic behaviour of cubic field $^5T_{2g}$ terms in lower symmetry. *J. Chem. Soc. A* **1967**, 442–447.
3. Long, G.J.; Baker, W.A. On the magnetic properties of some distorted octahedral high-spin iron(II) complexes. *J. Chem. Soc. A* **1971**, 2956–2959, doi:10.1039/J19710002956.
4. Kotani, M. On the magnetic moment of complex ions. (I). *J. Phys. Soc. Jpn.* **1949**, *4*, 293–297.
5. Abragam, A.; Pryce, M.H.L. The theory of paramagnetic resonance in hydrated cobalt salts. *Proc. Roy. Soc. A* **1951**, *206*, 173–191.
6. Stevens, K.W.H.; Pryce, M.H.L. On the magnetic properties of covalent XY_6 complexes. *Proc. Roy. Soc. A* **1953**, *219*, 542–555.
7. Figgis, B.N. The magnetic properties of transition metal ions in asymmetric ligand fields. Part 2.—Cubic field $^3T_2$ terms. *Trans. Faraday Soc.* **1961**, *57*, 198–203.
8. Figgis, B.N.; Lewis, J.; Mabbs, F.E.; Webb, G.A. The magnetic behaviour of cubic field $^3T_{1g}$ terms. *J. Chem. Soc. A* **1966**, 1411–1421.
9. Freedman, D.E.; Harman, W.H.; Harris, T.D.; Long, G.J.; Chang, C.J.; Long, J.R. Slow Magnetic Relaxation in a High-Spin Iron(II) Complex. *J. Am. Chem. Soc.* **2010**, *132*, 1224–1225.
10. Bar, A.K.; Pichon, C.; Gogoi, N.; Duhayon, C.; Ramasesha, S.; Sutter, J.-P. Single-ion magnet behaviour of heptacoordinated Fe(ii) complexes: On the importance of supramolecular organization. *Chem. Commun.* **2015**, *51*, 3616–3619.
11. Sakiyama, H. Theoretical equations of Zeeman energy levels for distorted metal complexes with $^5T_{2g}$ ground terms. *J. Math. Chem.* **2019**, *57*, 858–874.
12. White, A.P.; Robertson, K.N.; Cameron, T.S.; Liengme, B.V.; Leznoff, D.B.; Trudel, S.; Aquino, M.A.S. Synthesis and characterization of $[M(DMSO)_6][SnCl_6]$ complexes (M=Fe^{2+}, Co^{2+}, and Ni^{2+}) An old mystery solved. *Can. J. Chem.* **2007**, *85*, 372–378.
13. Szostak, E.; Migdał-Mikuli, A. Thermal analysis, phase transitions and molecular reorientations in $[Fe(OS(CH_3)_2)_6](ClO_4)_2$. *J. Therm. Anal. Calorim.* **2017**, *129*, 1151–1158.
14. Sakiyama, H.; Sudo, R.; Abiko, T.; Yoshioka, D.; Mitsuhashi, R.; Omote, M.; Mikuriya, M.; Yoshitake, M.; Koikawa, M. Magneto-structural correlation of hexakis-dmso cobalt(II) complex. *Dalton Trans.* **2017**, *46*, 16306–16314.
15. Sakiyama, H.; Abiko, T.; Ito, M.; Mitsuhashi, R.; Mikuriya, M.; Waki, K.; Usuki, T. Reversible crystal-to-crystal phase transition of an octahedral zinc(II) complex with six dimethylsulfoxide. *Polyhedron* **2019**, *158*, 494–498.
16. Sakiyama, H.; Shomura, K.; Ito, M.; Waki, K.; Yamasaki, M. The crystal structure of $[Mg(dmso)_6][BPh_4]_2$ and the formation mechanism of the conformer on the basis of conformational analysis. *Dalton Trans.* **2019**, *48*, 10174–10179.
17. Sakiyama, H.; Abiko, T.; Ito, M.; Mitsuhashi, R.; Mikuriya, M.; Waki, K. Conformational analysis of an octahedral zinc(II) complex with six dimethylsulfoxide. *Polyhedron* **2016**, *119*, 512–516.
18. Kahn, O. *Molecular Magnetism*; VCH: Weinheim, Germany, 1993.
19. Sakiyama, H. Theoretical equations of Zeeman energy levels for distorted metal complexes with $^3T_1$ ground terms. *Magnetochemistry* **2019**, *5*, 17.
20. Figgis, B.N.; Hitchman, M.A. *Ligand Field Theory and Its Application*; Wiley-VCH: Weinheim, Germany, 2000.
21. Schmidt, M.W.; Baldridge, K.K.; Boatz, J.A.; Elbert, S.T.; Gordon, M.S.; Jensen, J.H.; Koseki, S.; Matsunaga, N.; Nguyen, K.A.; Su, S.; et al. General atomic and molecular electronic structure system. *J. Comput. Chem.* **1993**, *14*, 1347–1363.
22. Gordon, M.S.; Schmidt, M.W. *Advances in Electronic Structure Theory*; Elsevier: Amsterdam, The Netherlands, 2005.
23. Tawada, Y.; Tsuneda, T.; Yanagisawa, S.; Yanai, T.; Hirao, K. A long-range-corrected time-dependent density functional theory. *J. Chem. Phys.* **2004**, *120*, 8425–8433.
24. Weigend, F.; Ahlrichs, R. Balanced basis sets of split valence, triple zeta valence and quadruple zeta valence quality for H to Rn: Design and assessment of accuracy. *Phys. Chem. Chem. Phys.* **2005**, *7*, 3297–3305.
25. Weigend, F. Accurate Coulomb-fitting basis sets for H to Rn. *Phys. Chem. Chem. Phys.* **2006**, *8*, 1057–1065.